communications earth & environment

Article

A Nature Portfolio journal

https://doi.org/10.1038/s43247-025-03079-2

Leveraging peri-urban forests to reduce temperature and air pollution-related urban mortality in European cities

Check for updates

Alessandro Anav[1], Maurizio Gualtieri[2], Beatrice Sorrentino[1], Ilaria D'Elia[1], Pierre Sicard[3,4], Elena Paoletti[5] & Alessandra De Marco[1,4]

Extreme temperatures and poor air quality contribute to premature mortality, increased hospital admissions and higher healthcare costs. As the majority of the world's population lives in cities, understanding how urban vegetation mitigates temperature and pollution hazards is essential for designing strategies to enhance urban resilience and reduce mortality. However, estimating the health benefits of urban greening is challenging due to the non-linear physical, chemical, and biological processes involved. Here we use a coupled climate-chemistry model to assess the impact of different peri-urban tree planting scenarios on temperature- and pollution-related mortality and their associated costs over three Euro-Mediterranean cities. We find that peri-urban greening primarily allows to reduce mortality from non-optimal temperatures and, to a lesser extent, air pollution, with effectiveness depending on the selected trees species and local meteorological and chemical conditions. This study provides methodological insights to guide urban planners in leveraging nature-based solutions effectively while avoiding adverse health effects from poor tree selection.

Every year, millions of people die worldwide from cardiovascular and respiratory diseases associated with exposure to high concentrations of surface air pollutants[1], mainly fine particulate matter ($PM_{2.5}$), nitrogen dioxide (NO_2) and tropospheric ozone (O_3)[2–11]. In Europe only, in 2022, the exposure to $PM_{2.5}$, NO_2, and O_3 resulted in 269,000, 66,000, and 81,000 deaths, respectively[12]. In addition to poor air quality, extreme temperatures, including heat waves and cold spells, further increase mortality and morbidity[13–16]. While European regulations on air pollutants began in the 1980s[17], heat-related mortality has become a major concern following the 70,000 excess deaths registered during the 2003 heatwave[18] and the recent record-breaking temperatures experienced during the summers of 2022 and 2023, which led to 61,672[19] and 47,690[20] heat-related deaths, respectively. Furthermore, because of the continuous emissions of greenhouse gases, climate projections indicate a general increase in temperatures along with a rise in the intensity, frequency, and duration of heat waves[21–24] with severe contribution to mortality[25,26] and catastrophic economic impacts[27–30]. Consequently, as nearly 50% of cities worldwide are exposed to elevated $PM_{2.5}$ and O_3 levels[31], nature-based solutions (NBS)[32,33] are receiving growing attention for their potential to prevent premature mortality, especially in densely populated areas[34,35]. In this context, green spaces and urban or peri-urban forests have emerged as crucial elements due to their ability to improve air quality[36,37], by capturing pollutants through dry deposition[38], and mitigate the urban heat island (UHI)[39,40] effects through heat absorption and evapotranspiration[41–43]. However, at the same time, the emission of biogenic volatile organic compounds (BVOCs) from vegetation, mainly isoprene and monoterpenes, can worsen air quality by contributing to the formation of secondary air pollutants[44,45].

While some studies have investigated the large-scale effects of land cover change on air quality[46–48] and quantified the role of urban vegetation in removing common surface air pollutants[42], to the best of our knowledge, no studies have simultaneously examined how different urban greening solutions affect UHI, air pollution, and the associated mortality. Due to the non-linear nature of the processes involved[49], the concentration of surface air pollutants cannot be quantified a priori. In addition, reductions in pollutant concentrations, resulting from changes in precursor emissions or in dry deposition due to differences in plant phenology[50] and rooting zone[51], could increase thermal stress on human health, potentially outweighing the benefits of improved air quality. Consequently, the effectiveness of urban

[1]Italian National Agency for New Technologies, Energy and Sustainable Economic Development (ENEA), Via Anguillarese 301, Rome, Italy. [2]Department of Earth and Environmental Sciences, Polaris Research Centre, University of Milano-Bicocca, Piazza della Scienza 1, 2016, Milano, Italy. [3]ACRI-ST, Sophia-Antipolis, France. [4]National Institute for Research and Development in Forestry Marin Drăcea (INCDS), Voluntari, Romania. [5]Research Institute on Terrestrial Ecosystems, National Research Council of Italy (CNR-IRET), Via Madonna del Piano 10, 50019 Sesto Fiorentino, Florence, Italy. e-mail: alessandro.anav@enea.it; maurizio.gualtieri@unimib.it

greening solutions can be thoroughly evaluated using complex coupled climate-chemistry models capable of simultaneously reproducing atmospheric dynamics and accounting for the formation, destruction, removal, and transport of pollutants in the atmosphere. However, despite advancements in computational power, performing city-scale simulations remains challenging due to the substantial computational resources required.

To assess the effects of peri-urban greening on the preventable mortality burden from non-optimal temperatures and air pollution, we propose two tree planting strategies in three European cities: Florence (Italy), Aix-en-Provence (France) and Zagreb (Croatia) (Fig. 1). These cities were chosen considering climatic and morphological conditions, as well as urban density and pollution levels. Specifically, we selected cities located in the Mediterranean basin, as this region is already highly vulnerable to the combined impacts of air pollution and climate change, with a further increase in heat-related mortality expected in the near future[52]. In addition, we chose cities located inland and surrounded by hills, which reduces air circulation and exacerbates air pollution. Besides, they lack sufficient space to develop parks or large urban forests. Finally, in these areas, pollutant levels consistently exceed the WHO (World Health Organization) thresholds established for health protection. For these reasons, assessing the role of different greening solutions in the selected areas provides valuable insights for urban planners.

For each city, we first identify the tree species that are well-adapted to local climate conditions and characterized by either high or low BVOCs emissions. We then run the WRF-Chem model, replacing a portion of the original land cover with the selected tree species and changing the biogenic emission factors accordingly. Comparing these simulations with a baseline experiment, representing the actual land cover conditions, and a simulation where the vegetation around the cities is completely removed, allows to evaluate the effectiveness of the planting scenarios in reducing mortality and associated costs, and to understand the mechanisms driving changes in atmospheric chemistry and physics. This study represents a significant advance in urban sciences, offering valuable insights into the benefits and challenges of selecting appropriate tree species for planting.

Changes in air pollutant concentration

The analysis presented in this section is based on seasonal means; however, as positive and negative anomalies tend to offset each other, we highlight that the effects of greening policies could be even more pronounced at the hourly scale. Results indicate that the removal of all urban and peri-urban vegetation consistently increases summertime daily mean surface O_3 concentrations in the three analyzed cities and their surrounding rural areas (Fig. 2). In Florence, we find a mean city-scale increase of 1.3 ppb (+2.8%), in Aix-en-Provence 1.2 ppb (+2.6%), while in Zagreb the effect is more pronounced (1.9 ppb, +4.3%) with a large portion of the city experiencing a mean rise exceeding 2 ppb (Fig. 2). This noticeable increment is primarily attributed to a substantial reduction in the dry deposition (Fig. S3), which is well known to serve as the primary sink of O_3 in near-surface air[38]. In particular, the removal of vegetation reduces the amount of O_3 entering the leaves through plant stomata; besides, the reduction of other non-stomatal deposition pathways, including uptake by leaf cuticles, branches or other woody surfaces, decreases the amount of O_3 removed by deposition, thereby enhancing the concentrations remaining in the atmosphere.

Considering the scenarios, planting species with high BVOC emissions is generally associated with increased dry deposition (Fig. S3), due to the larger stomatal conductance of the deciduous trees compared to the cropland or mixed forests of the baseline scenario. At the same time, the emissions of isoprene, monoterpenes and other important precursors for tropospheric O_3 are enhanced (Fig. S4). Conversely, selecting low-BVOC species for planting leads to a substantial reduction in isoprene emissions (Fig. S4). Interestingly, the results highlight that planting both high and low BVOC-emitting trees reduces the O_3 concentration. The most pronounced effect occurs in Florence (−0.8 ppb, −1.7%), where we observe a negligible difference between the two planting strategies. In Aix-en-Provence, planting low BVOC-emitting trees is slightly more effective at reducing O_3 compared to planting high-BVOC-emitting trees (−0.25 ppb vs. −0.18 ppb, −0.5 vs. −0.4%, respectively). On the other hand, in Zagreb, the high-BVOC-emitting trees do not produce any substantial change, while the low BVOC-emitting trees allow to reduce the mean O_3 concentration of −0.27 ppb (−0.6%).

Disentangling these counter-intuitive results, i.e., decreased ozone concentrations resulting from either increasing or reducing BVOC emissions, is complex, as several counteracting biosphere–atmosphere interaction pathways are involved. A recent study on the impacts of forestation-induced greening on ozone air quality in China shows that, through enhanced dry deposition combined with reduced turbulence and vertical transport below and near the tree canopy, afforestation can offset the effect of increased biogenic emissions[53]. Here, we hypothesize a similar

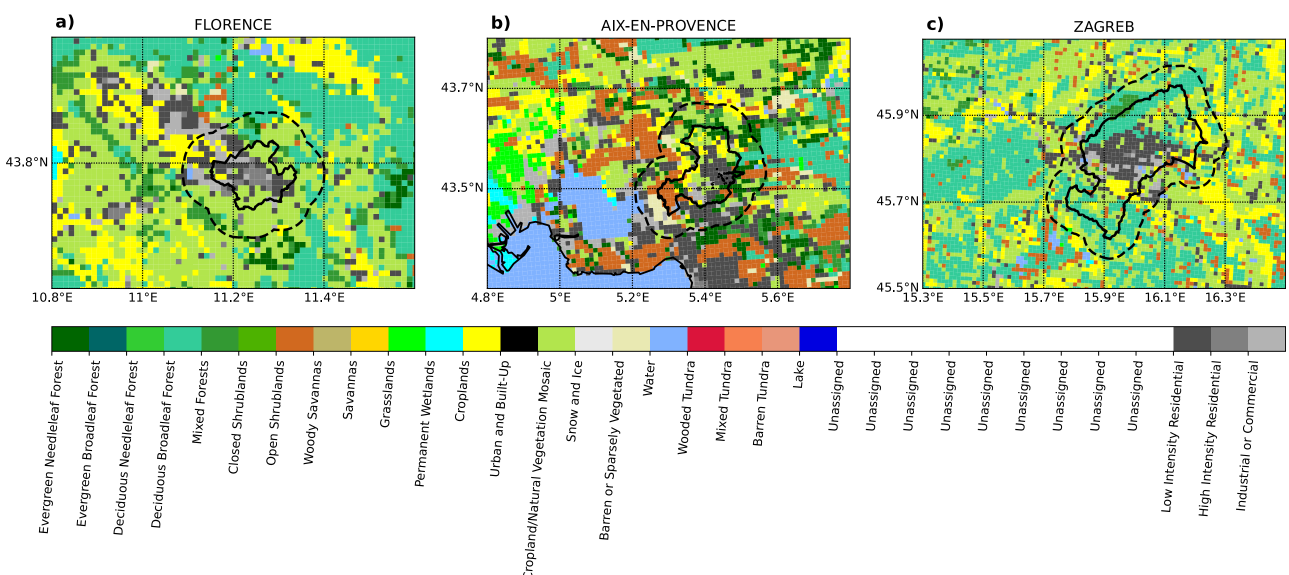

Fig. 1 | Spatial extension of dominant land-cover type. CORINE land use regrouped to the US Geological Survey (USGS) classes and interpolated to the 1 km WRF-Chem grids around the cities of **a** Florence, **b** Aix-en-Provence, and **c** Zagreb. The solid lines represent the city boundaries, while the dashed lines indicate the 5 km reference area around the city boundaries where we replaced the actual land cover, testing the effect of planting low and high-BVOC-emitting trees on heat- and pollution-related mortality.

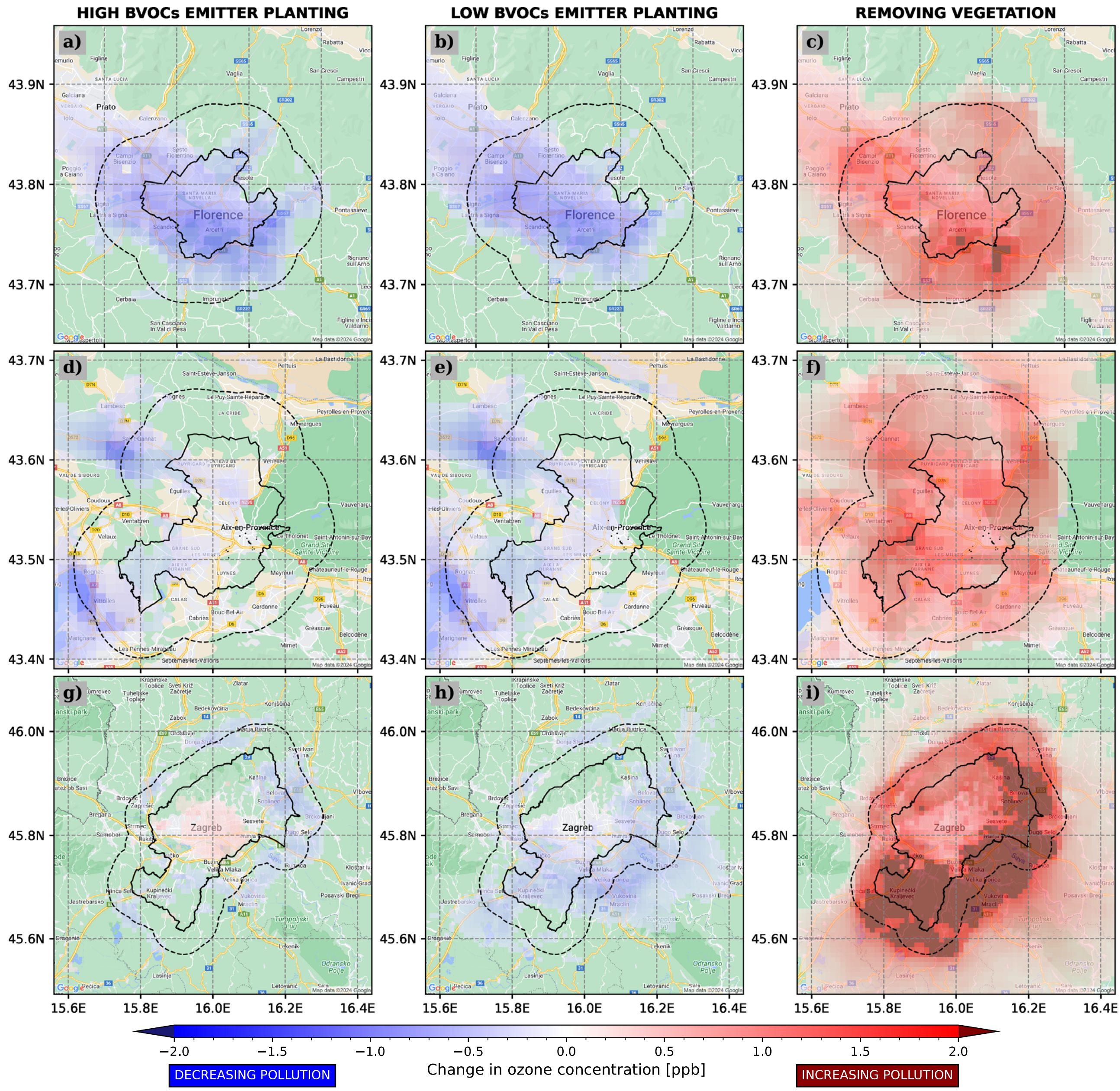

Fig. 2 | Changes in surface O_3 concentration considering different tree planting scenarios. Difference in mean summer O_3 concentration between the control run, which is intended to represent the actual land-cover conditions, and three different planting strategies for the cities of Florence (**a–c**), Aix-En-Provence (**d–f**), and Zagreb (**g–i**). The map was generated using Google Maps (Map data ©2024 Google).

mechanism, namely, the two proposed tree planting strategies suppress turbulence and vertical transport below and near the canopy, thereby reducing the downward mixing of ozone from the free troposphere to the surface. In addition, the non-linearity of the O_3–VOC–NO_x system indicates that, depending on the photochemical regime of the city of interest and particularly its NO_x levels, O_3 destruction can be achieved by either increasing or decreasing BVOC emissions[49].

Considering the aerosols, it is well recognized that the vegetation represents an important source of BVOCs, which are major precursors of secondary organic aerosols (SOA)[44]. Looking at fine particulate matter (Fig. S5), results indicate that removing vegetation reduces $PM_{2.5}$ concentrations, with a mean city-scale decrease of 1.3% in Florence, 2.2% in Aix-en-Provence, and 3.0% in Zagreb. These differences are primarily driven by reductions in precursor BVOCs emissions (Fig. S4) and changes in both wind speed and mixing depth. The changes in ventilation conditions depend on the decrease of the roughness length and surface friction, which strengthen the wind speed (Fig. S6); this, in turn, promotes the dispersion of fine particles outside the cities as well as their mixing and dilution in the planetary boundary layer (PBL). Conversely, planting high BVOCs emitters generally enhances the $PM_{2.5}$ concentration with a city-scale average of 0.80% in Florence and Aix-en-Provence, and 0.12% in Zagreb. In contrast, planting low BVOC-emitting species leads to a smaller increase in $PM_{2.5}$ (0.35% in Florence and 0.30% in Aix-en-Provence) and a slight reduction in Zagreb (−0.07%).

Changes in urban heat island intensity

The primary effect of land cover change on local climate is the modification of the different components of the surface energy balance[54]. These modifications lead to an alteration of the surface air temperature, as a consequence of both the change in the available energy at the soil level and the change in the way this energy is redistributed into the lower part of the PBL[55].

To quantify how the tree planting strategies affect the UHI intensity, we compare the distribution of daily summer maximum surface air temperatures between urban and rural areas for the three analyzed cities (Fig. 3). Looking at the control simulation, in Florence and Zagreb the UHI intensity is 1.1 and 0.54 K, respectively, while Aix-en-Provence does not show any UHI, with the temperature of rural area 0.3 K warmer than the urban area. The absence of the UHI in Aix-en-Provence can be attributed to the presence of extensive urban vegetation, which provides cooling through evapotranspiration, as well as the small city size characterized by narrow and shaded streets, which limit the amount of shortwave radiation reaching built surfaces, thereby reducing surface heating.

Considering Florence, our results indicate that the planting strategies do not produce any substantial change in the urban daily maximum surface air temperature, and the only notable observed difference, compared to actual land-cover conditions, is a slight reduction in UHI intensity (0.7 K) in the scenario where all the vegetation is replaced with bare ground. This decrease in UHI intensity is mostly related to a 0.4 K warming in the rural area caused by increased thermal radiation (Fig. S7). In fact, under bare ground conditions, the soil receives more radiation due to reduced vegetation shading, resulting in higher soil temperatures and, consequently, increased infrared radiation—the primary mechanism by which the soil transfers heat to the lower atmosphere. In addition, a reduction in latent heat flux (more than 30 W/m^2, Fig. S8) and an increase in sensible heat flux (>10 W/m^2, Fig. S9) produce drier and warmer conditions in the near-surface atmosphere. Similarly to Florence, in Aix-en-Provence and Zagreb, no noticeable changes are observed in the distribution of maximum temperature compared to the actual land-cover conditions.

These results demonstrate that the peri-urban land-cover changes have a limited impact on the maximum temperatures: in fact, the urban maxima are more strongly controlled by large-scale conditions and local insolation patterns than by advection of moisture and heat from rural areas. This finding is further supported by the mean hourly cycle of summer surface temperature (Fig. S10), which clearly underscores how vegetation removal consistently increases urban temperatures at night and in the late afternoon, while its impact during daytime hours remains minimal. In particular, the increased daytime thermal radiation (Fig. S11) is offset by an enhanced ground heat flux (Fig. S12), which drives energy transfer from the soil surface into deeper layers during the day. At night, this stored energy is released back toward the surface, warming the lower atmosphere through sensible heat flux (Fig. S13). Similarly, planting both low- and high-BVOC species leads to a cooling effect only outside of daytime hours (Fig. S10). This reinforces the conclusion that temperature maxima are primarily controlled by large-scale meteorological conditions, and that changes in vegetation type and cover have only a marginal effect. Nevertheless, planting strategies have a notable impact on the distribution of the minimum temperatures (Fig. S14), which typically occur at night (Fig. S10) and are more controlled by local conditions. Considering the analyzed cities, the minimum temperatures of rural areas are higher than the urban areas (Fig. S14) because of the release of the heat stored during the day by the soil and vegetation[41,56]. Our results highlight that planting strategies involving both high and low BVOC-emitting trees can slightly reduce the summer minimum temperatures in the three cities (Fig. S14), primarily due to the reduced release of heat from the soil as thermal radiation (Fig. S11), while the removal of the vegetation increases the temperature in both urban and rural areas. These results align well with a similar study, which showed that the strongest impact of greening is on the occurrence of tropical nights, while its effect on the maximum daily temperatures is marginal, although the total number of heat days and heat-wave days is slightly reduced when tree cover is increased[57].

Implications for mortality rates

Figure 4 clearly indicates how the removal of vegetation increases the number of attributable deaths across the analyzed cities, with a mean city-scale increase per 100,000 inhabitants of 13.0 (95% CI: 11.6–14.2) for Florence, 2.9 (95% CI: 2.1–3.3) for Aix-en-Provence, and 59.4 (95% CI: 45.3–72.8) for Zagreb. Excess mortality is primarily associated with an increase in the number of days when temperatures exceed (or fall below) the local maximum (or minimum) mortality temperature. While there is general agreement on this pattern, most of the additional deaths in Florence and Aix-en-Provence are attributed to warm temperatures, whereas in Zagreb, excess mortality is more strongly linked to cold days. On the other hand, the substantial O_3 reduction (Fig. 2) has a negligible effect, likely because the 8-h

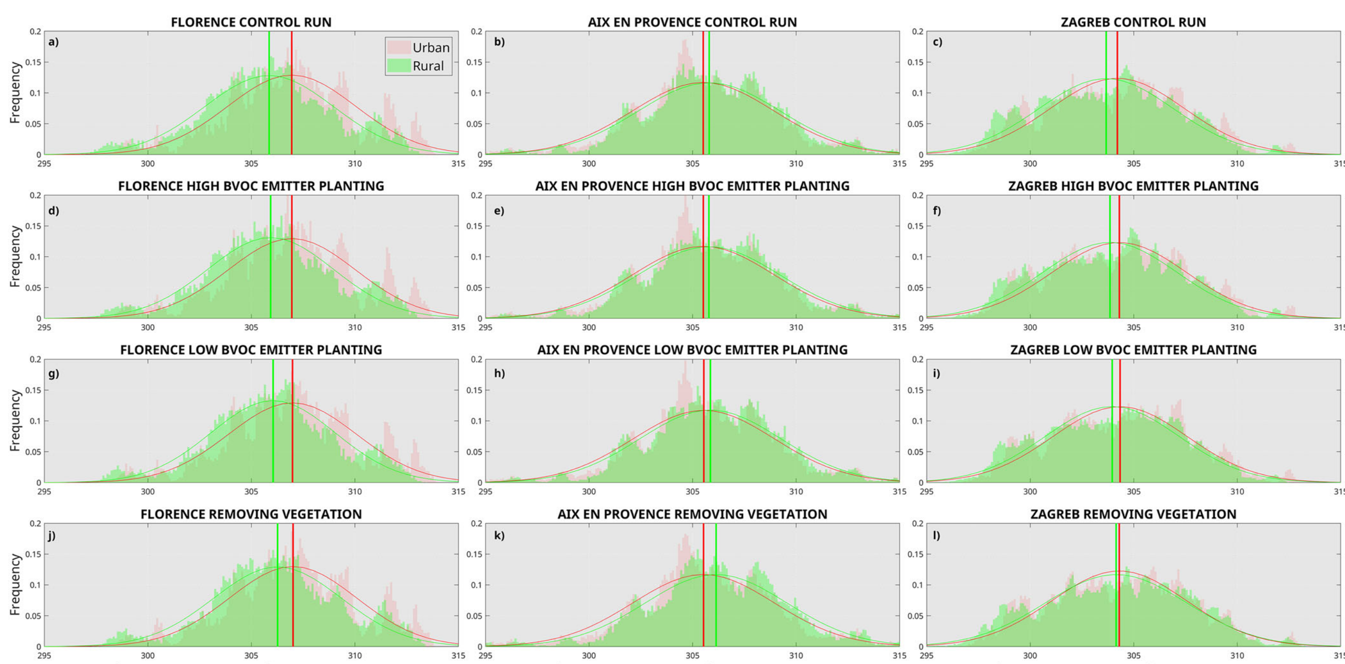

Fig. 3 | Distribution of daily maximum temperature from different tree planting scenarios. Probability density functions of summer daily maximum temperature for urban (red) and rural (green) areas around the three test cities of Florence (**a**, **d**, **g**, **j**), Aix-En-Provence (**b**, **e**, **h**, **k**) and Zagreb (**c**, **f**, **i**, **l**) computed from different tree planting strategies.

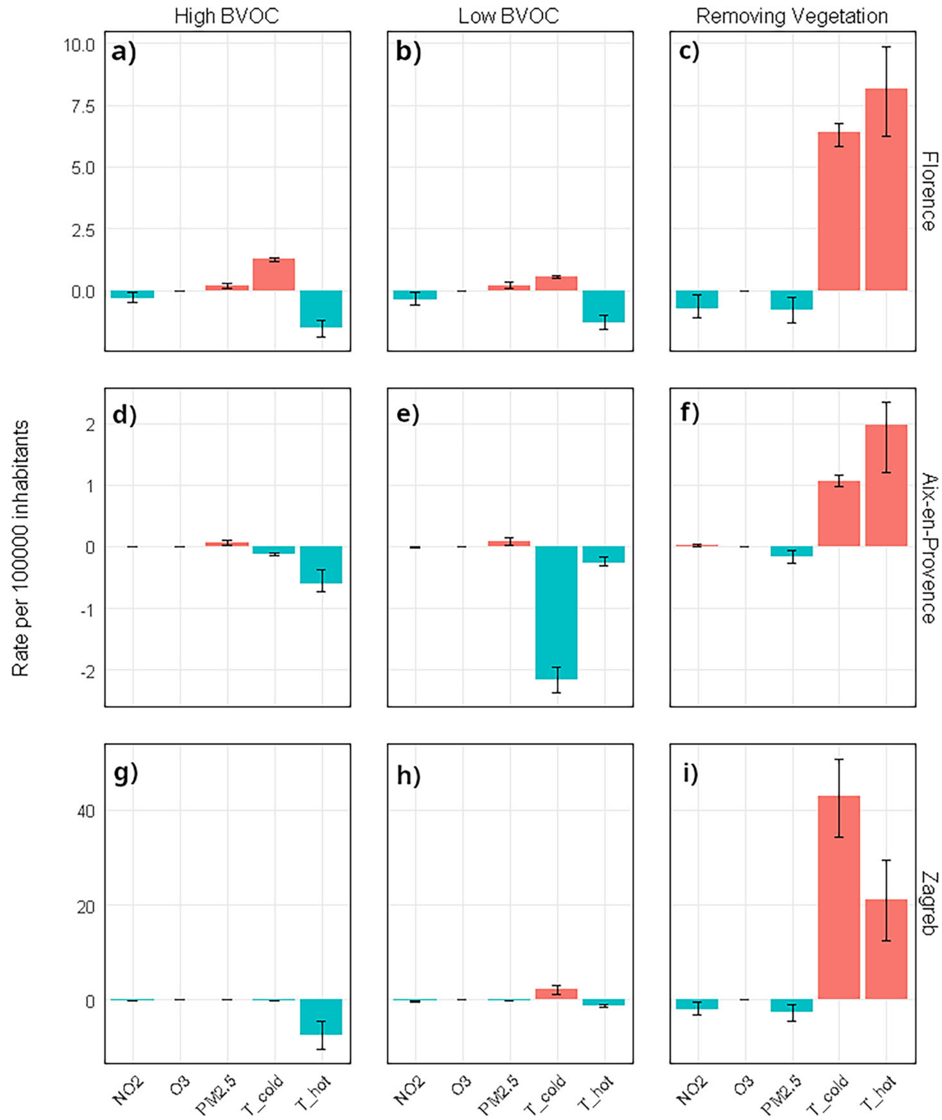

Fig. 4 | Changes in the number of attributable deaths considering different tree planting scenarios. Change in mortality rates due to nitrogen dioxide (NO_2), ozone (O_3), fine particulate ($PM_{2.5}$), cold (T_cold) and warm temperatures (T_hot) between the scenarios and the control run in the three analyzed cities of Florence (**a**, **b**, **c**), Aix-En-Provence (**d**, **e**, **f**) and Zagreb (**g**, **h**, **i**). Red columns represent increased mortality rates, while blue ones are associated with decreased mortality. Data are reported as mean values, with error bars representing the minimum and maximum associated with relative risk variability.

moving average concentrations are already below the harmful threshold of 30 ppb. Conversely, the decrease in $PM_{2.5}$ (Fig. S5) contributes to reducing the number of attributable deaths, as does the NO_2, at least in Florence and Zagreb. Nonetheless, the effects of air pollutants on attributable deaths are remarkably lower than those caused by non-optimal temperatures.

Considering the different scenarios, in Aix-en-Provence, planting low-emitting species remarkably reduces the mortality associated with cold temperatures. In this case, the total number of preventable deaths per 100,000 inhabitants due to temperature and air pollution is 2.4 (95% CI: 2.1–2.6), which is considerably larger than the 0.7 (95% CI: 0.5–0.8) achieved with high-emitting species. Similarly, in Florence, planting low-emitting species results in a reduction in avoidable deaths of 0.9 (95% CI: 0.5–1.2), primarily due to decreased mortality from high temperatures; this scenario is slightly more effective than the high-BVOC-emitting scenario, which leads to a decrease of 0.4 (95% CI: 0.1–0.7). Conversely, in Zagreb, the largest reduction in attributable deaths is achieved by planting high-emitting species, which primarily decrease the number of additional deaths caused by high temperatures, with a reduction of 7.7 (95% CI: 4.5–10.6) for 100,000 inhabitants. On the other side, planting low-emitting species results in a net increase of mortality equal to 0.6 (95% CI: 0.2–1.0).

Interestingly, considering the rate of attributable cases per square km of modified areas (Table S1), results underscore that the highest reduction in mortality rates is achieved planting low-emitting scenario in Aix-en-Provence, with an average rate of 0.25 (95% CI: 0.23–0.28) avoided deaths per newly afforested square km, followed by Zagreb under the high emitting scenario (0.17 avoided deaths, 95% CI 0.53–0.86).

According to the increased mortality burden, the scenarios without vegetation are also associated with higher costs. The highest values are found in Zagreb, where the associated economic value of health impacts ranges from €331 million to €708 million, followed by Florence with €240 million to €560 million, and finally Aix-en-Provence with €68 million to €158 million. (Table S2). In all scenarios, the highest costs are linked to non-optimal temperature-related mortalities. Regarding air pollution, the results indicate that cost reductions can be achieved in all cities by planting both high- and low-BVOC-emitting trees, primarily through a decrease in costs associated with NO_2, while $PM_{2.5}$ and O_3 show a mixed response depending on the city and scenario. It should also be noted that in this study, we did not account for all-cause mortality, indicating that peri-urban greening may lead to even greater reductions in mortality and costs.

Conclusions

Here, using a coupled climate-chemistry model, we propose two peri-urban tree planting solutions and assess their effectiveness in reducing temperature- and pollution-related mortality across three European cities. Our results indicate that peri-urban greening is more effective at lowering mortality from non-optimal temperatures than from air pollution.

Nevertheless, the benefits of increasing urban tree coverage on pollution-related mortality are well recognized: a recent study that examined 744 European cities[36] shows how, compared to the current tree cover, a 5% increase in tree canopy within each city would potentially prevent 4727 premature deaths (95% CI 2067–7475), while an increase of canopy cover of 30% could potentially prevent 11,974 premature deaths (95% CI 7775–14,390) each year.

Interestingly, a survey on different NBS to implement in Europe prioritized reducing air pollutants over mitigating the adverse effects of temperature[58], suggesting a lack of awareness among the European population about the actual health impacts of non-optimal temperatures. However, the wide latitudinal spread of the survey participants, with individuals from the Netherlands and the United Kingdom being less exposed to severe heat stress than those from southern European countries, likely influenced the results. In any case, considering both the effects of increasing urban tree coverage in reducing pollutant concentrations[36] and that future temperature-related mortality is projected to increase more than pollution-related mortality[52], decision-makers should adopt strong mitigation and adaptation measures to prevent loss of life associated with both non-optimal temperatures and air pollution.

Our results also highlight an intricate interplay between the emission and formation processes in controlling secondary air pollutant concentrations. For instance, considering the O_3 production, it increases with rising NO_x concentrations up to a certain threshold, beyond which additional NO_x begins to inhibit its formation; at this stage, the addition of VOCs stimulates O_3 production[49,59]. In urban environments, the O_3 formation is generally highly sensitive to the concentration of VOCs, being the nitrogen oxides present in abundance due to emissions from vehicles[60]. However, our results highlight that comparable improvements in air quality can be achieved through both increases and decreases in BVOC emissions, with Florence and Aix-en-Provence showing greater reductions in attributable deaths achieved by planting low-emitting species, whereas in Zagreb, by planting high-emitting species.

Overall, our results underscore that the benefits achievable through peri-urban vegetation vary among cities; therefore, the effects of different tree planting policies must be evaluated on a case-by-case basis. In other words, it is not straightforward to draw a general conclusion applicable to other cities with different climates and chemical regimes. Nevertheless, our results clearly indicate that increasing urbanization, especially when accompanied by the complete removal of urban and peri-urban vegetation, dramatically increases mortality burdens and associated costs.

In this context, advancements in computational power, along with the adaptability of the methodology used in this study to cities worldwide, make this research a valuable tool. In fact, in the near future, next-generation climate-chemistry models running on GPUs will enable accurate estimation of the minimum percentage of vegetation replacement that maximizes health benefits, allowing more precise scenario analyses and facilitating exploration of sensitivity to different tree species. Moreover, coordinated efforts among different modeling groups will enable the investigation of uncertainties in model parameterizations and assumptions. Thus, our insights, combined with emissions control strategies and complementary interventions (e.g., cold air corridors, green roofs), can help maximize public health benefits and enhance citizens' well-being, ultimately contributing to the development of more sustainable and climate-resilient cities.

Methods

Modeling urban climate and pollutant concentrations

The WRF-Chem model[61] (v 4.2.2) is applied in this study to produce detailed information on both air quality and meteorological conditions at urban scale. WRF-Chem is an online-coupled meteorology and chemistry regional model able to simulate, at the same time, the atmospheric dynamics and chemical transformation and transport of trace gases and aerosols.

A model configuration with three nested domains was adopted to accurately simulate the urban climate and pollutant concentrations in three sample cities: Florence (Italy), Aix-en-Provence (France), and Zagreb (Croatia) (Fig. S1). Initially, a broad domain (d01) covering Europe was configured with a 15 km horizontal resolution on a Lambert conformal grid. Subsequently, we used a finer domain (d02) of 5 km resolution centered on the Western Mediterranean Sea, and, finally, simulations were conducted at a 1 km resolution over the selected cities.

The WRF-Chem model provides various physical and chemical schemes. Key physical parameterizations include the rapid radiative transfer model (RRTM) for the short- and longwave radiation[62], the Mellor–Yamada–Janjic (MYJ) scheme for boundary layer processes[63], the Morrison two–moment scheme for the precipitation[64], and the Noah-MP Land Surface Model for surface—atmosphere interactions[65]. Regarding the atmospheric chemistry, MOZART (Model for OZone And Related chemical Tracers) is used to simulate gas-phase reactions[66], while MOSAIC (Model for Simulating Aerosol Interactions and Chemistry) accounts for aerosol dynamics[67]. The WRF/BEM building effect parameterization[68] is used to simulate the impacts of urban canopy on the urban climate. Relevant parameters for BEM (building energy model), including building height and other urban morphology parameters, were taken from the World Urban Database and Access Portal Tool (WUDAPT)[69] and additional data provided by the local municipalities. To provide WRF-Chem with proper information on the urban structure, land use data were adapted from the CORINE land cover inventory at a 100 m resolution.

The initial and boundary conditions of meteorological fields are updated every 3 h from the global reanalysis ERA5[70], while chemical initial and boundary conditions were provided by CAM-Chem[71]. Anthropogenic emissions, including all human activities like traffic, industries and agriculture, were derived from CAMS-GLOB-ANT[72], fire emissions were obtained from the FINN[73] inventory, while biogenic emissions were calculated online within WRF-Chem using the MEGAN[74] model. The simulations were conducted for the entire 2019 with a spin-up of 3 days. A detailed description of the model set-up and performances can be found in the validation paper[75].

Simulating different species-specific planting strategies

To investigate how urban and peri-urban forests influence the concentrations of surface air pollutants and the intensity of urban heat island, for each city four different numerical experiments were performed: (1) a control simulation relying on CORINE inventory to represent the actual land-cover conditions, (2) a high-BVOC emitters planting strategy where, starting from the present-day land cover conditions, we replaced 50% of the cropland/natural vegetation mosaic in a reference area obtained by widening the urban boundary by 5 km with *Quercus robur*, a species well adapted to live in the Mediterranean climate and characterized by high isoprene emissions rates[76], (3) a low BVOC emitters planting strategy where we plant *Pinus pinea* in Florence and Aix-en-Provence and *Pinus nigra* in Zagreb following the same procedure used before for the high BVOC emitters, and (4) an experiment where we replaced all the vegetation categories in the reference area of 5 km around the municipalities with bare ground. While planting high or low BVOC-emitting trees represent a concrete plans of action for cities to decrease the mortality following sound nature-based solutions, the latter experiment aims to quantify the contribution of current urban and peri-urban vegetation (i.e., grass, shrubs, and trees) in influencing the urban climate and air pollution. The spatial distribution of actual land cover, the city boundaries and the 5 km reference area around the city boundaries are shown in Fig. 1, while details on the land cover distribution of the scenarios can be found in Fig. S2.

The 50% threshold for replacing original vegetation was chosen to ensure that either low- or high-emitting trees become the dominant vegetation in the scenario simulations. Since the model weights all physical, chemical, and biological processes according to vegetation fraction, this threshold facilitates a clear depiction of the differences in dominant vegetation distribution among the scenarios, as shown in Fig. S2. Nevertheless, we underscore that the higher the percentage of replacement, the greater the resulting effects of peri-urban afforestation. However, due to the prohibitive computational times, we were unable to explore the sensitivity to the percentage of replaced vegetation; thus, we selected the lowest possible replacement percentage to ensure a sound nature-based solution, as replacing 100% of the original vegetation was considered unrealistic. Clearly, this approach represents one of several possible interventions. In the near future, advances in computational power will allow us to increase model resolution and test different planting strategies, including various tree species and fractions.

Like most of the chemical transport models (CTMs) and climate models, WRF-Chem typically relies on broad categories to describe the land use types (Fig. 1). Consequently, several modifications were made to allow the model to include species-specific trees. While in the physical component of the model, we just prescribed the vegetation fraction, with leaf area index (LAI), directly computed at run-time by the model, we adapted the MEGAN[74] model to take into account the biogenic emissions of specific trees. Emission factors for the selected species were retrieved from literature[76].

Urban heat island calculation

The urban heat island (UHI) is calculated from WRF-Chem simulated surface air temperature.

As the UHI is defined as the temperature difference between an urban area and a neighboring rural area, to identify the UHI, we firstly defined an area around the city boundaries[43,77]; to be consistent with the tree–planting strategies, we selected the same reference area obtained by extending outwards the urban boundary by 5 km. This allows identifying a ring equal to the urban area where to calculate the UHI (see Fig. 1). Then, we grouped all the grid points falling within this reference area, denoted by the dotted lines in Fig. 1, into two groups: grid points with an urban land use fraction above 0.95 are classified as urban areas, while grid points with a fraction of grass, shrubs, or trees above 0.95 are considered rural areas. Besides, to remove the effect of different elevations between grid points, urban and rural surface air temperatures were altitude adjusted using a constant moist lapse rate of 6.5 K/km, which is commonly used for height corrections[78–81]. Notably, other studies use a dry adiabatic lapse rate of 9.8 K/km[82,83], assuming an atmosphere with low water vapor content. For this reason, we also tested how different lapse rate assumptions affect our results and found that they have little impact on UHI intensity, due to the limited elevation difference between urban and rural locations. This result is consistent with a separate sensitivity analysis conducted in several cities in the United Kingdom[83]. Finally, we computed the probability distributions of summer daily minimum and maximum temperatures for both the urban and rural categories.

Quantification of mortality rates

The effect of the different peri-urban afforestation scenarios on total mortality for non-accidental causes was investigated according to the concentration–response function (CRF) approach[84,85]. Relative risk values for long-term exposure to O_3, NO_2, and $PM_{2.5}$ for the three cities were retrieved from the literature. Considering the NO_2 and $PM_{2.5}$, the meta-analyses from Boogard et al.[86] and Huangfu et al.[87] were selected as applicable to the geographical areas under evaluation. Similarly, the meta-analysis from ref. 88 is considered representative of mortality related to O_3 exposure. Considering the temperature-related mortality, we used different values of relative risk (RR) for Zagreb, Florence and Aix-en-Provence, selecting those specifically validated for the geographical areas under investigation. In particular, for Zagreb, we considered the values reported in ref. 25, while for Florence and Aix-en-Provence, those reported in ref. 16. The same approach was followed to define the representative minimum mortality temperatures (MMT) for the three cities, and we selected those reported by ref. 89. All the RRs selected for our analyses are reported in Supplementary Table S3.

The base mortality rates for the exposed populations were retrieved from the national statistical database for Florence (ISTAT.it) and from available regional or national descriptive information for Aix-En-Provence (www.insee.fr) and Zagreb (ourworldindata.org). The simulated mean daily concentrations of NO_2, $PM_{2.5}$ were averaged over the entire year, while for the O_3 we computed the 8-h moving average over the period May-October, using a threshold of non-effect set at 60 μg/m^3 (i.e., 30 ppb). In the case of temperature, the daily difference with respect to the MMT was calculated. These averages were then considered as representative of the long-term population exposure under the different scenarios. Attributable cases were then calculated according to both air pollutants[85] and temperature[90]. According to ref. 85 the following formula can be used to estimate the attributable cases of morbidity or mortality (E) to a pollutant:

$$E = \sum_{i=1}^{N} \beta_0 \times pop_i \times (e^{(\ln RR \times \Delta C_i)} - 1) \tag{1}$$

where β_0 represents the baseline mortality of the selected health effect for the city of interest, pop_i is the population in each grid cell (i) of the model, RR is the relative risk, while ΔC_i is the variation of the concentration of the selected pollutant respect to the control scenario concentration in each grid cell (i). ΔC_i was scaled according to the RR unit risk. The sum of the attributable cases from each grid represents the estimated attributable cases (E). For temperature, the difference between the minimum mortality temperature and the specific temperature for each grid cell (i) was first calculated to define the region of the RR curve to consider, below or over the MMT with its specific relative risk. Then, the difference between the control scenario and the alternative vegetation scenario was used to estimate the net effect of the vegetation.

Estimating the health burden costs

The economic value of life loss was determined using an approach widely recognized in the literature[91]. This approach requires to transform the number of attributable cases (of mortality or morbidity) into the number of years lost. A premature death due to environmental variables determines the loss of additional years of life according to the specific life expectancy. Therefore, the years of life lost (YOLLs) were calculated starting from the attributable mortality cases, according to the following equation:

$$YOLL = E^{*} AYL \tag{2}$$

where E represents the attributable mortality cases in each city and AYL is the average years lost estimated for each city from the European Environmental Agency database (https://discomap.eea.europa.eu/App/AQViewer/index.html?fqn=Airquality_Dissem.hra.countries_sel). The economic value of the YOLL for each pollutant and each city was then calculated by attributing an average value of a life year (VOLY) according to the following equation:

$$VOLY_i = VOLY_{\text{ref}} {}^{*} \left(\frac{GDP_i}{GDP_{eu}}\right)^{\beta} \tag{3}$$

where $VOLY_i$ represents the value of a life year for the specific EU region considered, namely Italy, France, or Croatia, $VOLY_{\text{ref}}$ is retrieved from literature[91], GDP_i is the gross domestic product of the three nations, GDP_{eu} is the gross domestic product of the whole European Union, and β represents the income elasticity and is equal to 0.8[70]. Both the GDP_i and GDP_{eu} were actualized to 2019, the year of the simulated scenarios.

Data availability

All the input data used in this study are freely available. The CORINE land cover data can be obtained from: https://land.copernicus.eu/en/products/corine-land-cover. The ERA5 initial and boundary meteorological conditions, provided by the European Centre for Medium-Range Weather Forecast (ECMWF), can be openly downloaded from the Copernicus climate data store: https://cds.climate.copernicus.eu/datasets/reanalysis-era5-pressure-levels?tab=download. The Community Atmosphere Model with Chemistry (CAM-chem) data for the chemical initial and boundary conditions are provided by the National Center for Atmospheric Research (NCAR) at https://www.acom.ucar.edu/cam-chem/cam-chem.shtml. Fire emission data are available at: https://www.acom.ucar.edu/Data/fire/, while anthropogenic emission data can be downloaded from: https://eccad.aeris-data.fr/2020/04/10/cams-glob-ant-v4-2-and-v4-2-r1-1-now-available/. The model outputs are analyzed with widely available tools in Python, NCL, and MATLAB. Enquiries about model output should be directed to the Corresponding author.

Code availability

The source code of the WRF-Chem model used in this study is publicly available via GitHub at the following link: https://github.com/wrf-model/WRF.

Received: 21 March 2025; Accepted: 1 December 2025;
Published online: 19 December 2025

References

1. Lelieveld, J., Evans, J. S., Fnais, M., Giannadaki, D. & Pozzer, A. The contribution of outdoor air pollution sources to premature mortality on a global scale. *Nature* **525**, 367–371 (2015).
2. Zhang, Q. et al. Transboundary health impacts of transported global air pollution and international trade. *Nature* **543**, 705–709 (2017).
3. Sigsgaard, T. & Hoffmann, B. Assessing the health burden from air pollution. *Science* **384**, 33–34 (2024).
4. Malashock, D. A. et al. Global trends in ozone concentration and attributable mortality for urban, peri-urban, and rural areas between 2000 and 2019: a modelling study. *Lancet Planet. Health* **6**, e958–e967 (2022).
5. Brauer, M. et al. Global burden and strength of evidence for 88 risk factors in 204 countries and 811 subnational locations, 1990–2021: a systematic analysis for the Global Burden of Disease Study 2021. *Lancet* **403**, 2162–2203 (2024).
6. Jerrett, M. et al. Long-term ozone exposure and mortality. *N. Engl. J. Med.* **360**, 1085–1095 (2009).
7. Chen, Z.-Y. et al. Population exposure to multiple air pollutants and its compound episodes in Europe. *Nat. Commun.* **15**, 2094 (2024).
8. Orellano, P., Reynoso, J., Quaranta, N., Bardach, A. & Ciapponi, A. Short-term exposure to particulate matter (PM10 and PM2.5), nitrogen dioxide (NO2), and ozone (O3) and all-cause and cause-specific mortality: Systematic review and meta-analysis. *Environ. Int.* **142**, 105876 (2020).
9. Achebak, H. et al. Geographic sources of ozone air pollution and mortality burden in Europe. *Nat. Med.* **30**, 1732–1738 (2024).
10. Nansai, K. et al. Consumption in the G20 nations causes particulate air pollution resulting in two million premature deaths annually. *Nat. Commun.* **12**, 6286 (2021).
11. Dedoussi, I. C., Eastham, S. D., Monier, E. & Barrett, S. R. Premature mortality related to United States cross-state air pollution. *Nature* **578**, 261–265 (2020).
12. European Environment Agency (EEA), Europe's air quality status 2023. EEA Briefings, 2023; Available at: https://www.eea.europa.eu/en/analysis/publications/europes-air-quality-status-2023.
13. Mora, C. et al. Global risk of deadly heat. *Nat. Clim. Change* **7**, 501–506 (2017).
14. Alho, A. M., Oliveira, A. P., Viegas, S. & Nogueira, P. Effect of heatwaves on daily hospital admissions in Portugal, 2000–18: an observational study. *Lancet Planet. Health* **8**, e318–e326 (2024).
15. Gasparrini, A. et al. Mortality risk attributable to high and low ambient temperature: a multicountry observational study. *Lancet* **386**, 369–375 (2015).
16. Masselot, P. et al. Excess mortality attributed to heat and cold: a health impact assessment study in 854 cities in Europe. *Lancet Planet. Health* **7**, e271–e281 (2023).
17. Crippa, M. et al. Forty years of improvements in European air quality: regional policy-industry interactions with global impacts. *Atmos. Chem. Phys.* **16**, 3825–3841 (2016).
18. Stott, P. A., Stone, D. A. & Allen, M. R. Human contribution to the European heatwave of 2003. *Nature* **432**, 610–614 (2004).
19. Ballester, J. et al. Heat-related mortality in Europe during the summer of 2022. *Nat. Med.* **29**, 1857–1866 (2023).
20. Gallo, E. et al. Heat-related mortality in Europe during 2023 and the role of adaptation in protecting health. *Nat. Med.* **30**, 3101–3105 (2024).
21. Perkins-Kirkpatrick, S. & Lewis, S. Increasing trends in regional heatwaves. *Nat. Commun.* **11**, 3357 (2020).
22. Fischer, E. M. & Schär, C. Consistent geographical patterns of changes in high-impact European heatwaves. *Nat. Geosci.* **3**, 398–403 (2010).
23. Schär, C. et al. The role of increasing temperature variability in European summer heatwaves. *Nature* **427**, 332–336 (2004).
24. Meehl, G. A. & Tebaldi, C. More intense, more frequent, and longer lasting heat waves in the 21st century. *Science* **305**, 994–997 (2004).
25. Martínez-Solanas, È. et al. Projections of temperature-attributable mortality in Europe: a time series analysis of 147 contiguous regions in 16 countries. *Lancet Planet. Health* **5**, e446–e454 (2021).
26. Masselot, P. et al. Estimating future heat-related and cold-related mortality under climate change, demographic and adaptation scenarios in 854 European cities. *Nat. Med.* **31**, 1294–1302. (2025).
27. García-León, D. et al. Current and projected regional economic impacts of heatwaves in Europe. *Nat. Commun.* **12**, 5807 (2021).
28. Sun, Y. et al. Global supply chains amplify economic costs of future extreme heat risk. *Nature* **627**, 797–804 (2024).
29. Huang, W. T. K. et al. Economic valuation of temperature-related mortality attributed to urban heat islands in European cities. *Nat. Commun.* **14**, 7438 (2023).
30. Newman, R. & Noy, I. The global costs of extreme weather that are attributable to climate change. *Nat. Commun.* **14**, 6103 (2023).
31. He, C. et al. Synergistic PM2.5 and O_3 control to address the emerging global PM2.5-O_3 compound pollution challenges. *Eco Environ. Health* **3**, 325–337 (2024).
32. Buma, B. et al. Expert review of the science underlying nature-based climate solutions. *Nat. Clim. Change* **14**, 402–406 (2024).
33. Seddon, N. Harnessing the potential of nature-based solutions for mitigating and adapting to climate change. *Science* **376**, 1410–1416 (2022).
34. Grimm, N. B. et al. Global change and the ecology of cities. *Science* **319**, 756–760 (2008).
35. Iungman, T. et al. Cooling cities through urban green infrastructure: a health impact assessment of European cities. *Lancet* **401**, 577–589 (2023).
36. Sicard, P. et al. Effect of tree canopy cover on air pollution-related mortality in European cities: an integrated approach. *Lancet Planet. Health* **9**, e527–e537 (2025).
37. Rojas-Rueda, D., Nieuwenhuijsen, M. J., Gascon, M., Perez-Leon, D. & Mudu, P. Green spaces and mortality: a systematic review and meta-analysis of cohort studies. *Lancet Planet. Health* **3**, e469–e477 (2019).
38. Clifton, O. E. et al. Dry deposition of ozone over land: processes, measurement, and modeling. *Rev. Geophys.* **58**, e2019RG000670 (2020).
39. Oke, T. R. The energetic basis of the urban heat island. *Q. J. R. Meteorol. Soc.* **108**, 1–24 (1982).
40. Xu, C. et al. Can improving the spatial equity of urban green space mitigate the effect of urban heat islands? An empirical study. *Sci. Total Environ.* **841**, 156687 (2022).
41. Zhao, L., Lee, X., Smith, R. B. & Oleson, K. Strong contributions of local background climate to urban heat islands. *Nature* **511**, 216–219 (2014).

42. Gong, C., Xian, C., Wu, T., Liu, J. & Ouyang, Z. Role of urban vegetation in air phytoremediation: differences between scientific research and environmental management perspectives. *npj Urban Sustain.* **3**, 24 (2023).
43. Yang, M. et al. Mitigating urban heat island through neighboring rural land cover. *Nat. Cities* **1**, 522–532 (2024).
44. Tsigaridis, K., Lathiere, J., Kanakidou, M. & Hauglustaine, D. Naturally driven variability in the global secondary organic aerosol over a decade. *Atmos. Chem. Phys.* **5**, 1891–1904 (2005).
45. Cao, J., Situ, S., Hao, Y., Xie, S. & Li, L. Enhanced summertime ozone and SOA from biogenic volatile organic compound (BVOC) emissions due to vegetation biomass variability during 1981–2018 in China. *Atmos. Chem. Phys.* **22**, 2351–2364 (2022).
46. Fu, Y., Tai, A. P. & Liao, H. Impacts of historical climate and land cover changes on fine particulate matter (PM 2.5) air quality in East Asia between 1980 and 2010. *Atmos. Chem. Phys.* **16**, 10369–10383 (2016).
47. Yang, W. & Jiang, X. Evaluating the influence of land use and land cover change on fine particulate matter. *Sci. Rep.* **11**, 17612 (2021).
48. Wu, S., Mickley, L. J., Kaplan, J. O. & Jacob, D. J. Impacts of changes in land use and land cover on atmospheric chemistry and air quality over the 21st century. *Atmos. Chem. Phys.* **12**, 1597–1609 (2012).
49. Monks, P. S. et al. Tropospheric ozone and its precursors from the urban to the global scale from air quality to short-lived climate forcer. *Atmos. Chem. Phys.* **15**, 8889–8973 (2015).
50. Anav, A. et al. The role of plant phenology in stomatal ozone flux modeling. *Glob. Change Biol.* **24**, 235–248 (2018).
51. Anav, A. et al. Sensitivity of stomatal conductance to soil moisture: implications for tropospheric ozone. *Atmos. Chem. Phys.* **18**, 5747–5763 (2018).
52. Pozzer, A. et al. Atmospheric health burden across the century and the accelerating impact of temperature compared to pollution. *Nat. Commun.* **15**, 9379 (2024).
53. Liu, Z. et al. Co-benefit of forestation on ozone air quality and carbon storage in South China. *Nat. Commun.* **16**, 2429 (2025).
54. Findell, K. L. et al. The impact of anthropogenic land use and land cover change on regional climate extremes. *Nat. Commun.* **8**, 989 (2017).
55. Bright, R. M. et al. Local temperature response to land cover and management change driven by non-radiative processes. *Nat. Clim. Change* **7**, 296–302 (2017).
56. Zhou, J., van der Molen, M. & Teuling, A. Contrasting below-and above-canopy climate regulation services of a temperate forest during heatwaves. *Agric. For. Meteorol.* **366**, 110485 (2025).
57. Bügelmayer-Blaschek, M., Züger, J. & Tötzer, T. Assessing the potential of urban wide greening for climate-resilience: the example of Vienna. *Sustain. Futures* **9**, 100532 (2025).
58. Pröbstl-Haider, U., Wanner, A., Feilhammer, M., Mostegl, N. & Dabrowska, K. The right fit: acceptance of nature-based solutions across European cities. *Landsc. Urban Plan.* **252**, 105189 (2024).
59. Madronich, S. Ethanol and ozone. *Nat. Geosci.* **7**, 395–397 (2014).
60. Beekmann, M. & Vautard, R. A modelling study of photochemical regimes over Europe: robustness and variability. *Atmos. Chem. Phys.* **10**, 10067–10084 (2010).
61. Grell, G. A. et al. Fully coupled “online” chemistry within the WRF model. *Atmos. Environ.* **39**, 6957–6975 (2005).
62. Mlawer, E. J., Taubman, S. J., Brown, P. D., Iacono, M. J. & Clough, S. A. Radiative transfer for inhomogeneous atmospheres: RRTM, a validated correlated-k model for the longwave. *J. Geophys. Res. Atmos.* **102**, 16663–16682 (1997).
63. Janjić, Z. I. The step-mountain eta coordinate model: Further developments of the convection, viscous sublayer, and turbulence closure schemes. *Mon. Weather Rev.* **122**, 927–945 (1994).
64. Morrison, H., Thompson, G. & Tatarskii, V. Impact of cloud microphysics on the development of trailing stratiform precipitation in a simulated squall line: Comparison of one-and two-moment schemes. *Mon. Weather Rev.* **137**, 991–1007 (2009).
65. Li, J. et al. Global evaluation of the Noah-MP land surface model and suggestions for selecting parameterization schemes. *J. Geophys. Res. Atmos.* **127**, e2021JD035753 (2022).
66. Emmons, L. K. et al. Description and evaluation of the Model for Ozone and Related chemical Tracers, version 4 (MOZART-4). *Geosci. Model Dev.* **3**, 43–67 (2010).
67. Zaveri, R. A., Easter, R. C., Fast, J. D. & Peters, L. K. Model for simulating aerosol interactions and chemistry (MOSAIC). *J. Geophys. Res. Atmos.* **113**, D13204 (2008).
68. Salamanca, F., Krpo, A., Martilli, A. & Clappier, A. A new building energy model coupled with an urban canopy parameterization for urban climate simulations—part I. formulation, verification, and sensitivity analysis of the model. *Theor. Appl. Climatol.* **99**, 331–344 (2010).
69. Ching, J. et al. WUDAPT: An urban weather, climate, and environmental modeling infrastructure for the Anthropocene. *Bull. Am. Meteorol. Soc.* **99**, 1907–1924 (2018).
70. Hersbach, H. et al. The ERA5 global reanalysis. *Q. J. R. Meteorol. Soc.* **146**, 1999–2049 (2020).
71. Tilmes, S. et al. Description and evaluation of tropospheric chemistry and aerosols in the Community Earth System Model (CESM1. 2). *Geosci. Model Dev.* **8**, 1395–1426 (2015).
72. Soulie, A. et al. Global anthropogenic emissions (CAMS-GLOB-ANT) for the Copernicus atmosphere monitoring service simulations of air quality forecasts and reanalyses. *Earth Syst. Sci. Data Discuss.* **2023**, 1–45 (2023).
73. Wiedinmyer, C. et al. The Fire INventory from NCAR (FINN): a high resolution global model to estimate the emissions from open burning. *Geosci. Model Dev.* **4**, 625–641 (2011).
74. Guenther, A. et al. The model of emissions of gases and aerosols from nature version 2.1 (MEGAN2. 1): an extended and updated framework for modeling biogenic emissions. *Geosci. Model Dev.* **5**, 1471–1492 (2012).
75. Anav, A. et al. Meteorological, chemical and biological evaluation of the coupled chemistry-climate WRF-Chem model from regional to urban scale. An impact-oriented application for human health. *Environ. Res.* **257**, 119401 (2024).
76. Karl, M., Guenther, A., Köble, R., Leip, A. & Seufert, G. A new European plant-specific emission inventory of biogenic volatile organic compounds for use in atmospheric transport models. *Biogeosciences* **6**, 1059–1087 (2009).
77. Valmassoi, A. & Keller, J. D. How to visualize the urban heat island in gridded datasets? *Adv. Sci. Res.* **18**, 41–49 (2021).
78. Dutra, E. et al. Environmental lapse rate for high-resolution land surface downscaling: an application to ERA5. *Earth Space Sci.* **7**, e2019EA000984 (2020).
79. Vargas, N. & Magaña, V. Climatic risk in the Mexico City metropolitan area due to urbanization. *Urban Clim.* **33**, 100644 (2020).
80. Bushenkova, A., Soares, P. M., Johannsen, F. & Lima, D. C. Towards an improved representation of the urban heat island effect: a multi-scale application of XGBoost for Madrid. *Urban Clim.* **55**, 1016 (2024).
81. Lauwaet, D. et al. High resolution modelling of the urban heat island of 100 European cities. *Urban Clim.* **54**, 101850 (2024).
82. Fenner, D., Holtmann, A., Meier, F., Langer, I. & Scherer, D. Contrasting changes of urban heat island intensity during hot weather episodes. *Environ. Res. Lett.* **14**, 124013 (2019).
83. Goddard, I. L. & Tett, S. F. How much has urbanisation affected United Kingdom temperatures?*Atmos. Sci. Lett.* **20**, e896 (2019).
84. Héroux, M.-E. et al. Quantifying the health impacts of ambient air pollutants: recommendations of a WHO/Europe project. *Int. J. Public Health* **60**, 619–627 (2015).

85. Orru, H. et al. Impact of climate change on ozone-related mortality and morbidity in Europe. *Eur. Respir. J.* **41**, 285–294 (2013).
86. Boogaard, H. et al. Long-term exposure to traffic-related air pollution and non-accidental mortality: a systematic review and meta-analysis. *Environ. Int.* **176**, 107916 (2023).
87. Huangfu, P. & Atkinson, R. Long-term exposure to NO2 and O3 and all-cause and respiratory mortality: A systematic review and meta-analysis. *Environ. Int.* **144**, 105998 (2020).
88. Sun, H. Z. et al. Cohort-based long-term ozone exposure-associated mortality risks with adjusted metrics: a systematic review and meta-analysis. *Innovation* **3**, 100246 (2022).
89. Tobías, A. et al. Geographical variations of the minimum mortality temperature at a global scale: a multicountry study. *Environ. Epidemiol.* **5**, e169 (2021).
90. Armstrong, B. et al. Longer-term impact of high and low temperature on mortality: an international study to clarify length of mortality displacement. *Environ. Health Perspect.* **125**, 107009 (2017).
91. Holland, M. Cost-benefit analysis of final policy scenarios for the EU Clean Air Package. Corresponding to IIASA TSAP report no.11, Version 2a. Report to European Commission DG Environment, http://ec.europa.eu/environment/air/pdf/TSAP%20CBA.pdf (2014).

Acknowledgements
This work was made in the framework of the Research Group 8.04.00 "Air Pollution and Climate Change" and under the Working Party 8.04.05 "Ground-level ozone" of the International Union of Forest Research Organizations (IUFRO). This work was carried out with the contribution of the LIFE financial instrument of the European Union in the framework of the AIRFRESH project "Air pollution removal by urban forests for a better human well-being" (LIFE19 ENV/FR/000086). E.P. acknowledges the project funded under the National Recovery and Resilience Plan (NRRP), Mission 4 Component 2 Investment 1.4—Call for tender No. 3138 of 16 December 2021, rectified by Decree n.3175 of 18 December 2021 of Italian Ministry of University and Research funded by the European Union—NextGenerationEU; Project code CN_00000033, Concession Decree No. 1034 of 17 June 2022 adopted by the Italian Ministry of University and Research, CUP B83C22002930006 Project title "National Biodiversity Future Center—NBFC" Spoke 5. The computing resources and the related technical support used for this work have been provided by CRESCO/ENEA-GRID high-performance computing infrastructure and its staff.

Author contributions
A.A. coordinated the study and designed the scenarios with the help of A.D.M., B.S., P.S., and E.P. A.A. also performed the simulations and analysis. M.G. and I.dE. contributed to the computation of attributable deaths and economic assessment. The paper was written by A.A. with contribution from all authors.

Competing interests
The authors declare no competing interests.

Additional information
Supplementary information The online version contains supplementary material available at https://doi.org/10.1038/s43247-025-03079-2.

Correspondence and requests for materials should be addressed to Alessandro Anav or Maurizio Gualtieri.

Peer review information *Communications Earth & Environment* thanks Jingwei Zhou and the other, anonymous, reviewer(s) for their contribution to the peer review of this work. Primary Handling Editors: Martina Grecequet. A peer review file is available.